Development of instability and turbulence in overturning lee waves: the map of different scenarios in Re–Pr space

S N Yakovenko

Khristianovich Institute of Theoretical and Applied Mechanics, SB RAS, Novosibirsk, Russia

Email: yakovenk@itam.nsc.ru

Abstract. Scenarios of the transition to turbulence in overturning lee waves generated by the two-dimensional obstacle in a stably stratified flow have been explored by visualization of velocity and scalar (density) fields, with analysis of spanwise spectra. The results are obtained by numerical solution of the continuity, Navier–Stokes and scalar equations for stratified fluid with the Boussinesq approximation, for varied Reynolds and Prandtl numbers relating to tank experiments, situations in atmosphere and oceans. Based on the computed data, the dependence of the most unstable perturbation wavelength on Reynolds and Prandtl numbers is derived.

1. Introduction

The results of scanning in the space of physical parameters (Reynolds number Re = UH/ν, Prandtl number Pr = ν/κ) are presented for instability and turbulence development scenarios in overturning internal lee waves generated by the two-dimensional cosine obstacle of height H in a stably stratified flow with the constant values of inflow density gradient and velocity U. Such a phenomenon is studied by visualization of velocity and density fields, with analysis of spectra obtained from DNS/LES data at $10^2 \le \mathrm{Re} \le 10^4$, $1 \le \mathrm{Pr} \le 700$, relating to tank experiments [1-3], atmospheric and oceanic situations.

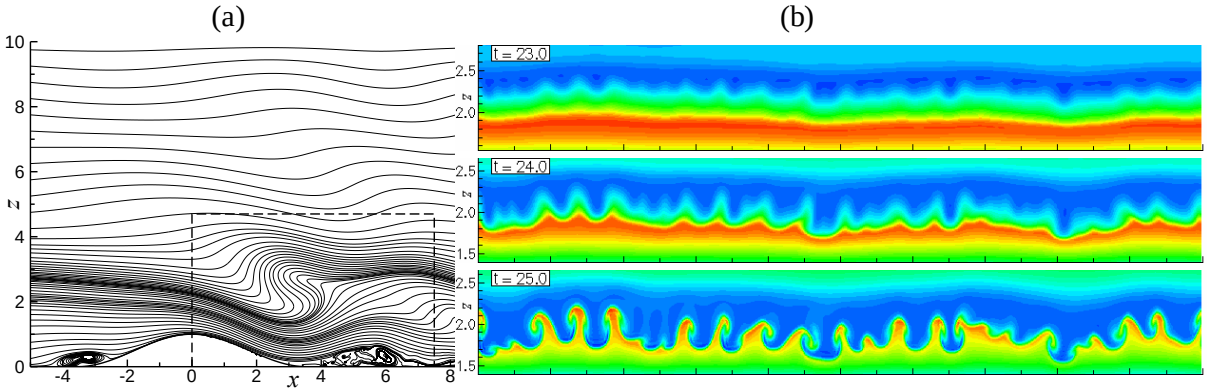

Figure 1. Pathlines, $t = 17.5$, $y = 0$ (a); density contours, $x = 2.5$ (b) in DNS at Re = 4000, Pr = 1.

The single case (Re = 4000, Pr = 1) was recently examined by DNS in [4,5] (figure 1). The grid resolution was sufficient to capture the fine-scale transition processes studied in [4] and the subsequent

developed turbulence discussed in [5]. For this set of parameters, secondary instability of the density field arising after wave overturning reveals a range of spanwise modes. The smallest mode ($\lambda_y \sim 0.5H$) represents oscillations of Rayleigh–Taylor instability (RTI), growing and resulting in convective mushroom-like structures with associated Kelvin–Helmholtz instability rolls. At late transition times, the smaller-scale vortices transform into the larger structures, and another noticeable mode ($\lambda_y \sim 2.5H$) is dominant when the large-scale toroidal vortex structures become evident [4]. This large-scale mode can be associated with the most unstable perturbation of the initial two-dimensional vortex pair in the wave-overturning place [4,5] and has also been detected in [2,3,6]. For higher Pr, the earlier and faster RTI growth with smaller-scale structures is observed in LES with Pr = 700 [7].

The more comprehensive study can be performed, with variation of physical/numerical parameters and conditions of computations: in particular, by means of multiple runs with varied Reynolds and Prandtl/Schmidt numbers. Reduction of Re (e.g. runs at Re = 2000, 1000, 500, 200, etc.) will allow us to even further refine the resolution due to larger relative values of Kolmogorov microscale η/H at smaller Reynolds numbers, thus to obtain better statistics in the turbulent patch. Another aim is to see the Re effect on transition details and quasi-steady turbulence. Runs at varied Re may give the light on the 'critical' Re value (Re_1) for onset of instability. This means that at $\mathrm{Re} < \mathrm{Re}_1$ all perturbations introduced in the region of internal wave overturning (e.g. white-noise seeding) will decay with time, and no structure will appear and transit to turbulence. On the other hand, at $\mathrm{Re} > \mathrm{Re}_2$ and depending on the grid resolution $\Delta x/H$, the DNS or implicit LES approach may become inadequate (as shown, e.g. by high-wavenumber parts of spectra), and for parameterization of smaller eddies of sub-grid scales (SGS) we will need then to introduce the SGS model. At Pr = 1, it is evident that $\mathrm{Re}_2 > 4000$ [4,5], so extra runs at larger Reynolds numbers, e.g. at $\mathrm{Re} = 10^4$ as in [1,3,8], would be of interest.

The aim of the Pr variation between 1 and 700 is to find the 'critical' values too, in particular, for DNS limitation, $\mathrm{Pr}_2(\Delta x)$ (for instance, at Re = 4000 we have $1 < \mathrm{Pr}_2 < 700$ for the resolution used in [4,5]), and approach to real situations: (1) non-isothermal atmosphere (Pr ~ 1), (2) non-isothermal water reservoir with Pr ≈ 7 at normal temperature, (3) salted water in ocean estuaries (Pr ≈ 700). It could be also interesting to address the dependence on Froude number and geometry of the obstacle, however, such an issue has already been explored in various experimental and numerical studies (e.g. in [1,8]). Moreover, from the point of view of flow physics and relevance for applications, dependence on values of Re and Pr seems to be more crucial.

2. Governing equations

The continuity, the Navier–Stokes and density equations for stratified fluid with the Boussinesq approximation are written in [4,5], as well as details of their realization.

3. Results and discussion

DNS results with fixed Pr = 1 at lower Re value (than in [4,5]) show that, for instance, for Re = 1000 (figures 2–5) multiple peaks in spanwise spectra ($0.6H < \lambda_y \leq 2.0H$) occur during perturbation growth at $25 < t < 40$. The most unstable perturbation wavelength corresponding to the RTI mode during the exponential growth stage ($30 < t < 35$) is $\lambda_y \approx 1.1H$ according to figures 4–5. The large-structure mode $\lambda_y \approx 3.3H$ arises during the turbulent patch stage at $t > 48$. The larger RTI structures (in comparison with the Re = 4000 case in [4,5]) evidently occur due to stronger viscosity/diffusion effects. These effects also cause delay of the instability and turbulence development, and smaller density drop between heavier and lighter fluid tongues (figure 3).

For Re = 500, one can find (figure 6) almost persistent dominance of the spectra peak with wavelength $\lambda_y \approx 2.0H$ (corresponding to the late RTI growth at $45 \leq t \leq 50$), as well as two weaker peaks with $\lambda_y \approx 0.9H$ at $45 \leq t \leq 60$ and $\lambda_y \approx 3.3H$ at $t > 48$. For both cases, Re = 500 and 1000 (as well as for Re = 4000 studied in [1,2]) one can see the large-structure enlargement with time growth.

For Re = 200, the spanwise instability magnitude is quite low (not visible in density contours) and does not lead to turbulence development, i.e. the critical value is within $200 < \mathrm{Re}_1 < 500$ at Pr = 1.

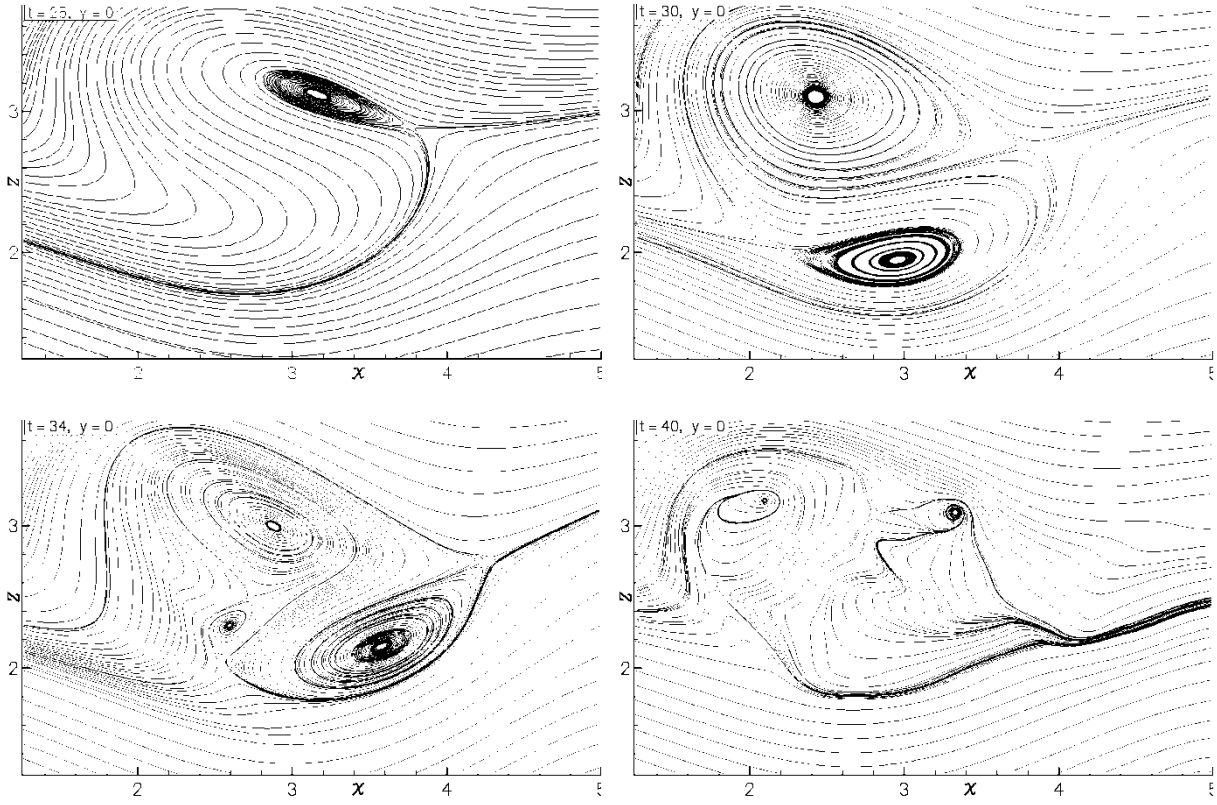

Figure 2. Instantaneous pathlines at Re = 1000, Pr = 1 for $t = 25, 30, 34, 40$ and $y = 0$.

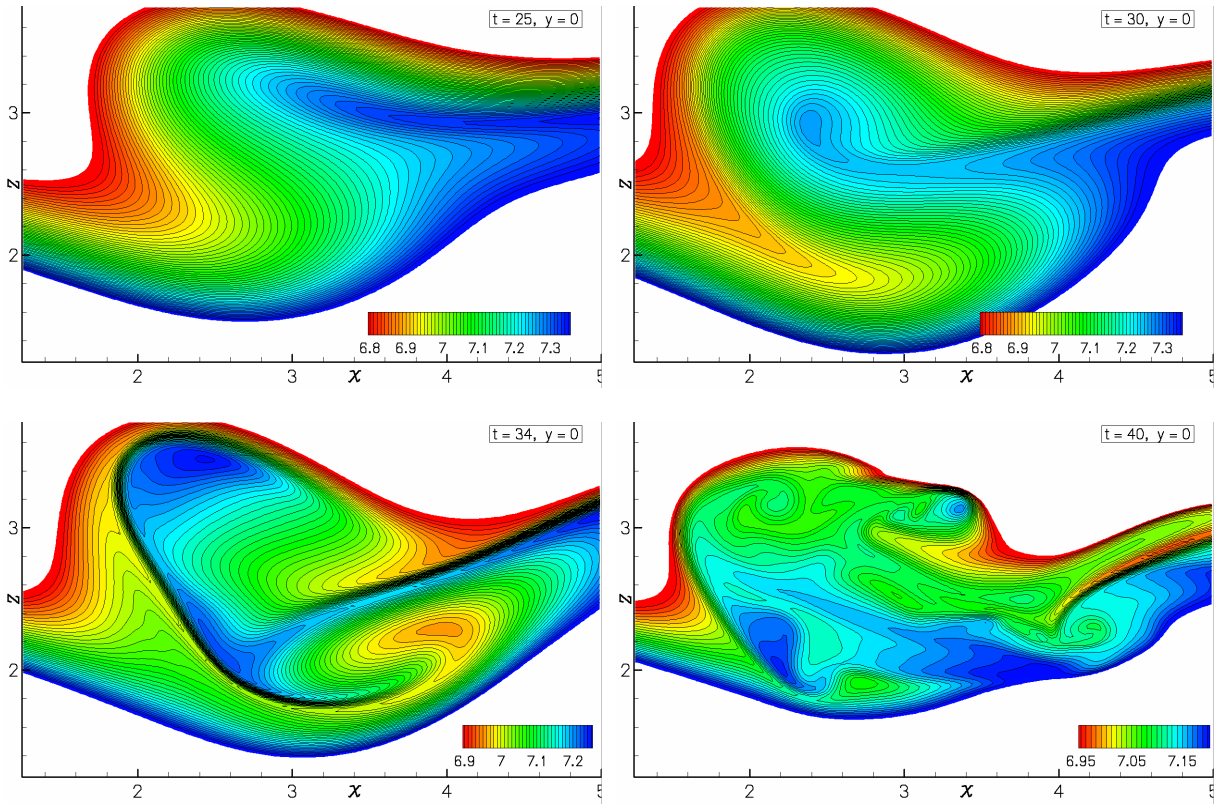

Figure 3. Instantaneous density contours at Re = 1000, Pr = 1 for $t = 25, 30, 34, 40$ and $y = 0$.

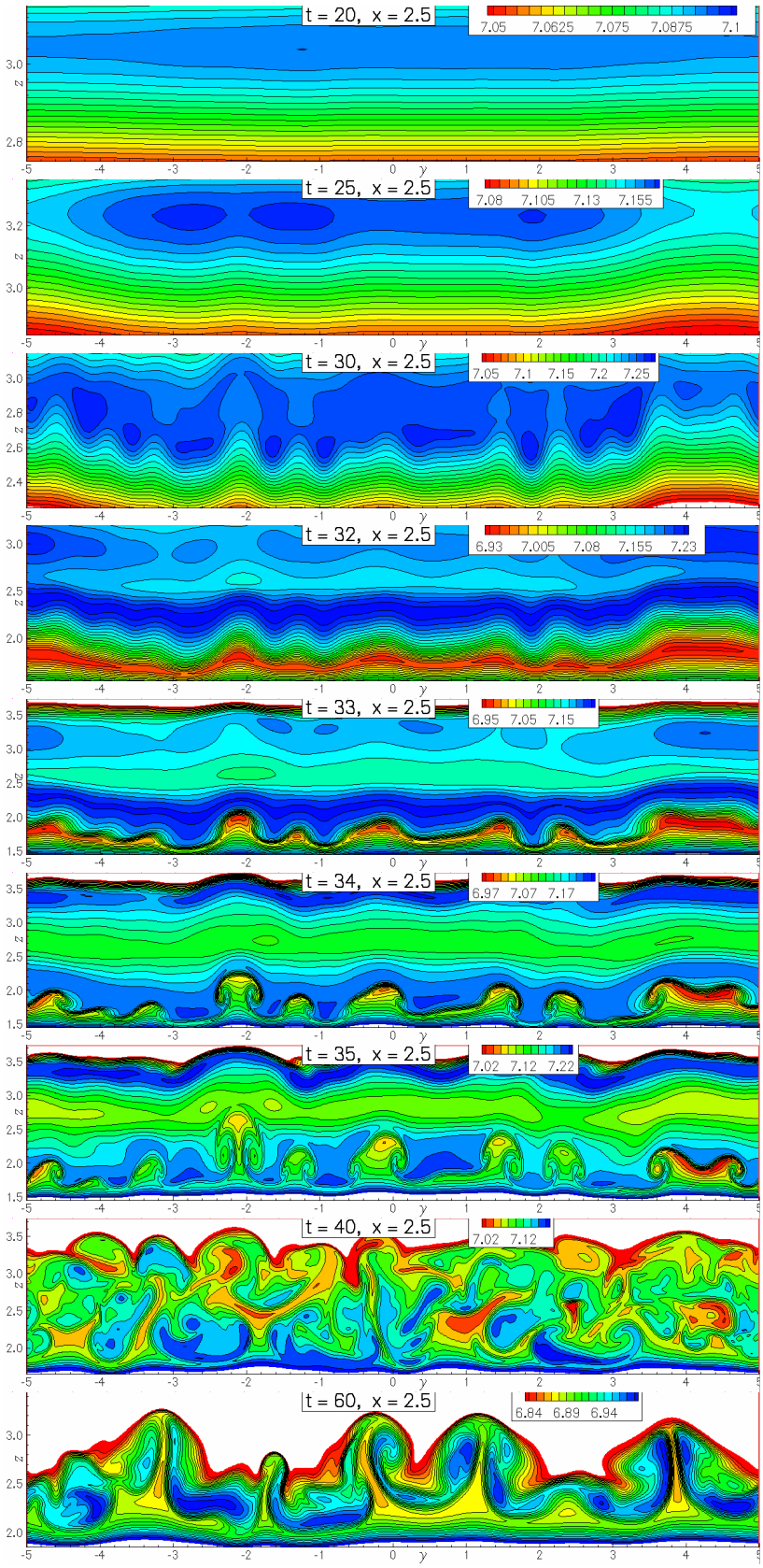

Figure 4. Instant density contours at Re = 1000, Pr = 1 ($t = 20, 25, 30, 32, 33, 34, 35, 40, 60, x = 2.5$).

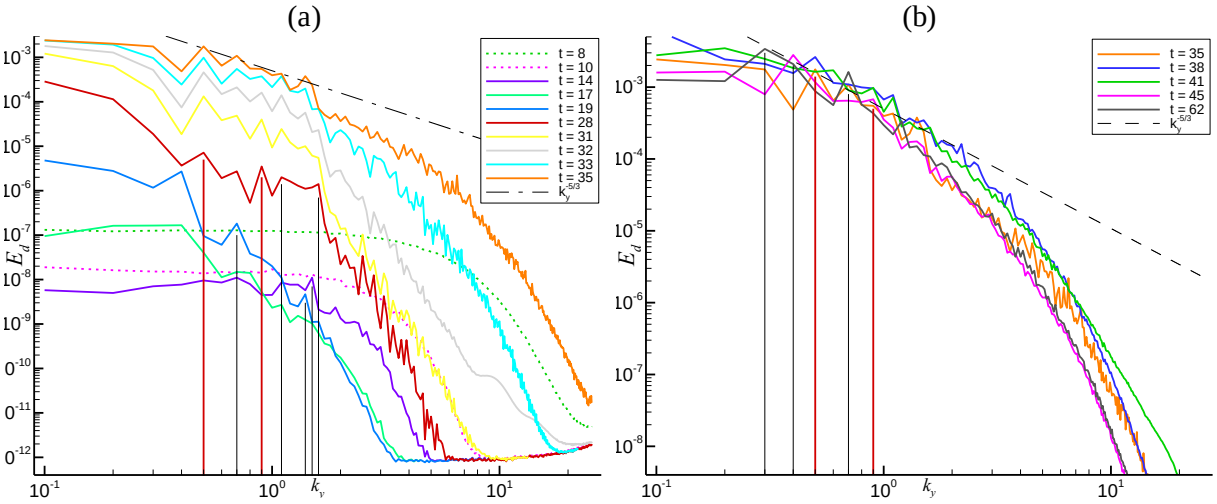

Figure 5. Spanwise spectra of scalar variance at Re = 1000, Pr = 1 (averaged at $1.25 \le x \le 5.00$ and $1.25 \le z \le 3.75$) during: (a) white-noise perturbation decay (dashed lines) and RTI growth (solid lines), (b) transition to quasi-steady turbulence (with rough relaxation to a single line).

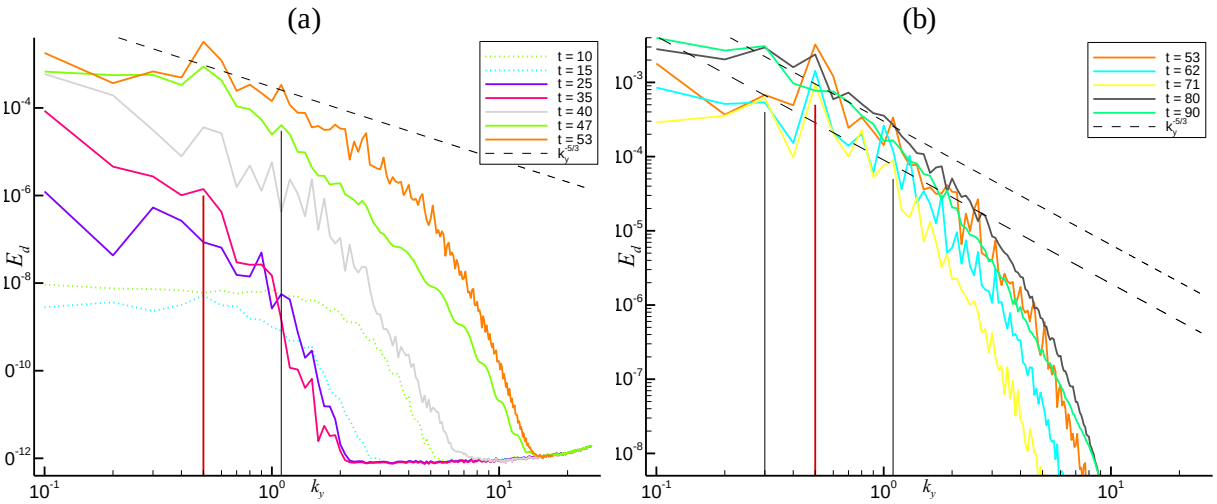

Figure 6. The same as in figure 5 for Re = 500, Pr = 1.

For Re = 10^4, the numerical noise becomes evident at large-wavenumber parts of spectra at late times corresponding to turbulent stages where the inertial range ($k^{-5/3}$) should be followed by larger slopes at higher k corresponding to dissipative ranges for both velocity and scalar spectra. In contrast, after the inertial range at $0.5 < k_y < 2.5$, we observe lower spectra slopes ($\sim k^{-1}$) at higher wave numbers $2.5 < k_y < 10$ (figure 7) which indicates an excessive spurious numerical noise appearing because of poor resolution (or absence of SGS models to suppress such a noise). Therefore, the second critical value is within $4\ 000 < \mathrm{Re}_2 < 10\ 000$ at Pr = 1, i.e. someone has to apply finer grids or LES techniques at Re > 4 000 to predict the small-scale flow features adequately.

In contrast to the Pr = 1 case, runs with the higher value Pr = 700 at Re = 200 do show the RTI growth with the most unstable perturbation wavelength $\lambda_y \approx 2.0H$ (figures 8 and 9), where the scalar spectra at the developed turbulent stage ($t > 60$) reveal not only the inertial range ($k^{-5/3}$), but also the viscous-convective range (k^{-1}) at higher wave numbers. The latter confirms the Batchelor's theory for Pr >> 1, whereas measurements could not capture this fine effect [9]. Note that we should be cautious here since this may be also affected by the density field under-resolution which seems to yield the same effect of smaller spectra slopes for high-wavenumber parts of spectra (figure 7).

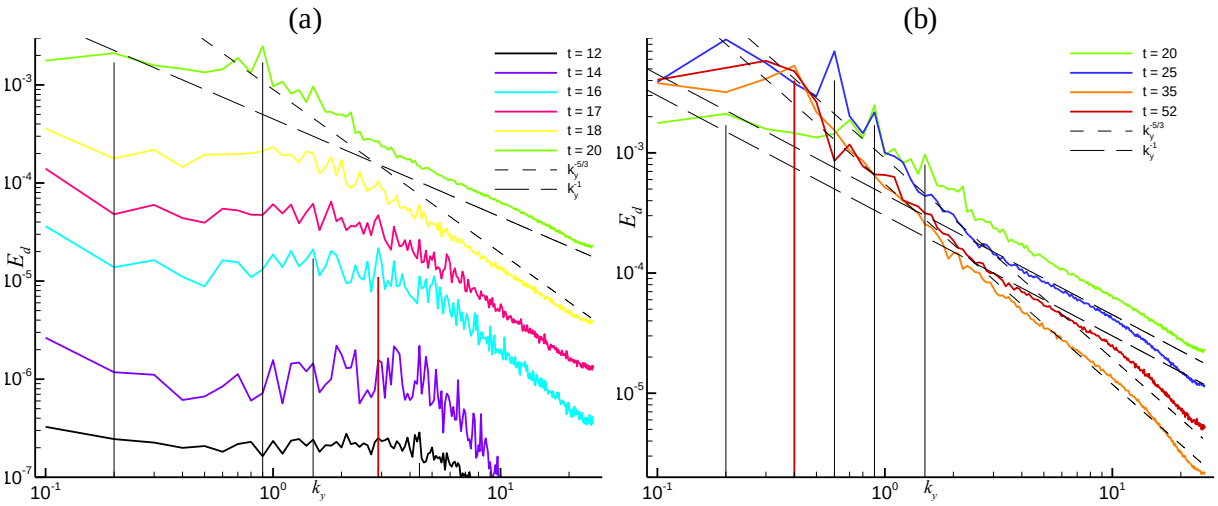

Figure 7. The same as in figure 5 for Re = 10^4, Pr = 1.

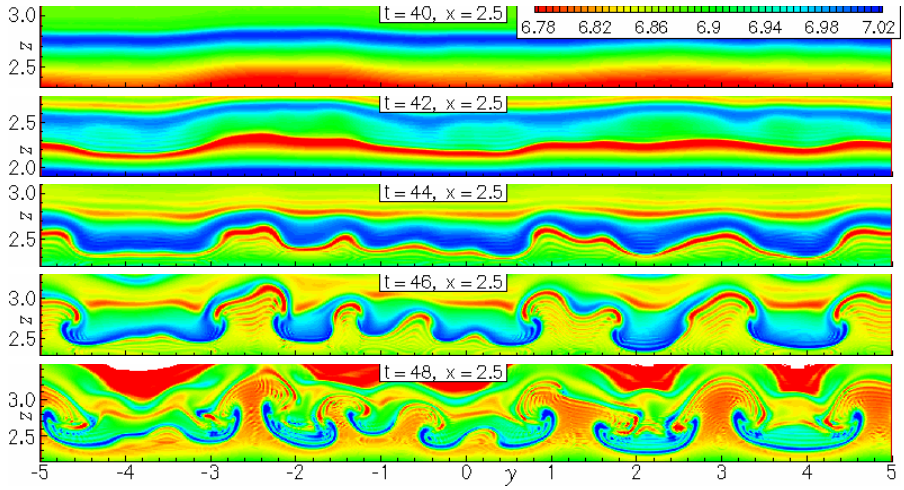

Figure 8. Instantaneous density contours at Re = 200, Pr = 700 for t = 40, 42, 44, 46, 48 and x=2.5.

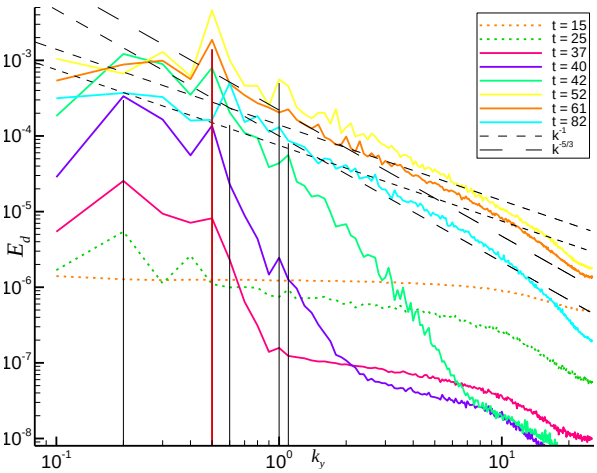

Figure 9. Spanwise spectra of scalar fluctuation variance for Re = 200 and Pr = 700 (averaged at $1.25 \le x \le 5.00$, $1.25 \le z \le 3.75$).

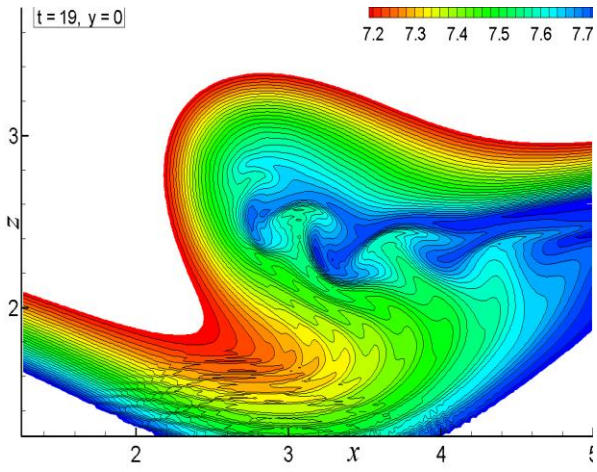

Figure 10. Instantaneous contours of density for Re = 4000, Pr = 7 (t = 19, y = 0), to be compared with figure 3 for Re = 1000, Pr = 1 (t = 25, 30).

For intermediate value Pr = 7, we still observe the transition to turbulence at low Reynolds number Re = 200 due to the RTI growth (which occurs quite late), in contrast to the case of Pr = 1. Note that at Pr = 7 the first critical value is within $100 < \mathrm{Re}_1 < 200$, whereas the second critical value is within $2000 < \mathrm{Re}_2 < 4000$, since the numerical density-field noise affects the high-wavenumber part of spanwise scalar spectra starting from Re ~ 4000 (and for Re = 2000 such an effect is not visible).

It is surprising that for Re = 4000 and Pr = 7 the RTI periodicity is seen not only along the span, but also in the streamwise direction as shown by visualization of density contours at $y = 0$ (figure 10). The similar effects are observed for $\mathrm{Re} = 10^4$ and Pr = 1. Although, in both cases we have the under-resolved density field resulting in excessive numerical noise, this evidence may still indicate another route of instability growth than the one discussed in [1] with quasi-two-dimensional structures.

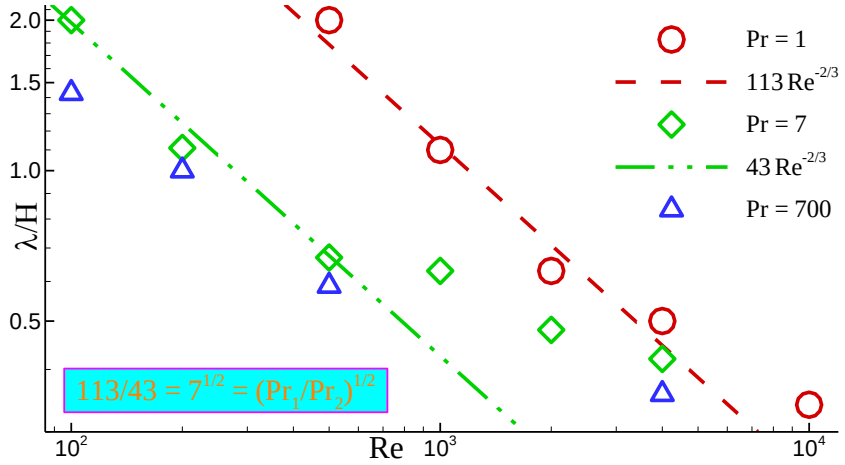

Figure 11. The map for the most unstable perturbation wavelength in the Re–Pr space.

The results can be summarized in figure 11 where the most unstable perturbation wavelength deduced from density snapshot visualizations and spectra peak analysis is given by symbols (each relates to one computation at different Re or/and Pr). One can see that the analytical expression [10]

$$\lambda = \lambda' = 4\pi H[(2\Delta\rho_H/\Delta\rho)(\mathrm{F}_H)^2\mathrm{Re}^{-2}]^{1/3}$$

(red dashed line in figure 11) written in dimensionless form [1] at Pr = 1 with the typical density drop, $\Delta\rho \approx 10^{-3}\Delta\rho_H$, between the layers of heavier and lighter fluids related to earlier RTI stages is satisfied. For arbitrary Pr values, the updated relation, $\lambda = f(\mathrm{Pr})\lambda'$, is next suggested according to figure 11 where $f(\mathrm{Pr}) \to \mathrm{const}$ at $\mathrm{Pr} \to \infty$ and $f(\mathrm{Pr}_1) > f(\mathrm{Pr}_2)$ at $\mathrm{Pr}_1 < \mathrm{Pr}_2$. In particular, the power-law function, $f(\mathrm{Pr}) \sim \mathrm{Pr}^{-1/2}$, may be valid for, at least, relatively low values between Pr ~ 1 and Pr ~ 10.

Note that the results at Pr = 700 are heavily affected by under-resolution of the density field, even at lower value of Re = 200. As the result, the numerical wiggles can be seen in growing mushroom-like structures (figures 8 and 10), and the numerical dissipation effect is a possible reason of obvious over-prediction of the most unstable perturbation wavelength (figure 11), as well as the SGS diffusion effect in the case of LES computation at Re = 4000 and Pr = 700.

4. Concluding remarks

The results of scanning in the space of Reynolds and Prandtl numbers for scenarios of the transition to turbulence in overturning internal lee waves generated by the two-dimensional obstacle in a stably stratified flow have been presented. The instability and turbulence development has been studied by visualization of velocity and density fields, with analysis of spanwise spectra obtained from numerical simulation data at $10^2 \le \mathrm{Re} \le 10^4$, $1 \le \mathrm{Pr} \le 700$.

The range of Prandtl numbers corresponds to heat stratification in the atmosphere (Pr ~ 1), reservoirs (Pr ~ 7) and to salted water diffusion (Pr ~ 700), whereas the range of Reynolds numbers

corresponds to the one in towing-tank measurements [1–3] and concurrent simulations [6,8]. The real atmospheric and oceanic flows have actually much higher levels of Re ~ $10^7 \div 10^{10}$. Nevertheless, as soon as we have quite high Re values with the fully developed turbulence at late stages (as a result of internal lee wave breaking), the behavior of the resulting turbulent patch is essentially the same regardless of transition routes and Re values, due to the well-known Reynolds number independence principle. So both laboratory and numerical experiments [1-8], as well as the present computations at Re ~ $10^2 \div 10^4$ replicate well the much higher Re situations in real geophysical conditions, except for the instability development stage. The latter may indeed have various scenarios with different structures from the zoo of instabilities at different Re. Nevertheless, the map of instability growth scenarios proposed here gives a hint to real flows and allows us to extrapolate results to geophysical situations with Re ~ $10^7 \div 10^{10}$, in particular, for the wavelength of the most unstable perturbation of RTI type which is proportional to $\mathrm{Re}^{-2/3}$ and falls with Pr values as $\mathrm{Pr}^{-1/2}$.

Acknowledgements
The author thanks Prof I.P. Castro and Dr T.G. Thomas for help in studies of breaking internal lee waves. The work was performed with use of the Iridis3 and Iridis4 computing resources at the University of Southampton.

References
[1] Castro I P and Snyder W H 1993 *J. Fluid Mech.* **255** 195–211
[2] Eiff O F and Bonneton P 2000 *Phys. Fluids* **12** 1073–86
[3] Eiff O, Huteau F and Tolu J 2005 *Dyn. Atmos. Oceans* **40** 71–89
[4] Yakovenko S N, Thomas T G and Castro I P 2014 *J. Fluid Mech.* **760** 466–93
[5] Yakovenko S N, Thomas T G and Castro I P 2011 *J. Fluid Mech.* **677** 103–33
[6] Gheusi F, Stein J and Eiff O F 2000 *J. Fluid Mech.* **410** 67–99
[7] Yakovenko S N, Thomas T G and Castro I P 2014 *Progress in Turbulence V: Proc. of the iTi Conf. in Turbulence, 2012* ed A Talamelli et al. Springer Proceedings in Physics vol 149 (Springer International Publishing) pp 233–36
[8] Paisley M F and Castro I P 1996 *Dyn. Atmos. Oceans* **23** 309–19
[9] Warhaft Z 2000 *Annu. Rev. Fluid Mech.* **32** 203–40
[10] Youngs D L 1984 *Physica* D **12** 32–44